Received: 2 December 2024 | Revised: 14 January 2025 | Accepted: 10 February 2025

DOI: 10.1002/cac2.70006

CANCER COMMUNICATIONS Open Access

LETTER TO THE JOURNAL

Neoadjuvant chemotherapy plus anlotinib in the treatment of resectable head and neck squamous cell carcinoma: A pilot phase II trial

Head and neck squamous cell carcinoma (HNSCC) continues to be a major global health challenge, with limited survival improvements for patients with locally advanced (LA) or recurrent (R) disease [1]. Anlotinib, a novel orally administered small-molecule tyrosine kinase inhibitor (TKI) developed in China, targets a wide range of receptor tyrosine kinases (RTKs) [2]. Our previous studies have also manifested that anlotinib remarkably inhibited the proliferation of HNSCC cells both in vitro and in vivo, and presented promising clinical antitumor efficacy and tolerable safety profile in patients with oral squamous cell carcinoma (OSCC) [3, 4]. This prospective trial was designed to evaluate the clinical efficacy and safety of anlotinib combined with paclitaxel and cisplatin (TP) neoadjuvant therapy in patients with resectable HNSCC. Additionally, the mechanisms underlying the effects of anlotinib and neoadjuvant chemotherapy on HNSCC were investigated through spatial transcriptomics (STs) and multiplex immunohistochemistry (mIHC).

Between October 2022 and May 2023, 20 resectable HNSCC patients were enrolled (median age, 55; range, 27-73). Baseline demographics and disease characteristics are detailed in Supplementary Tables S1-S2. All patients received 3 cycles of neoadjuvant therapy, followed by surgery in 17 and maintenance therapy in 16. No patients were lost to follow-up (study flowchart in Figure 1A). After neoadjuvant therapy, 95.0% (19/20) achieved partial response (PR), and 5.0% (1/20) achieved complete response (CR), with an Objective response rate (ORR) of 100% (95% confidence interval [CI], 83.2-100). Figure 1B shows the waterfall plot of tumor size changes. Surgical resection was performed in 17 patients (LA, 12; R, 5) with a 100% R0 resection rate, one patient declined surgery due to financial constraints and the other two did not want to perform surgery as their tumors had almost regressed. Postoperative pathological efficacy (Supplementary Table S3) showed pathological complete response (pCR) and major pathological response (MPR) in 7 patients each (41.2%; 95% CI, 18.4-67.1). Among 11 with positive cervical lymph nodes, 6 achieved pCR (54.5%; 95% CI, 23.4-83.3). Imaging and pathological data of patient #14 with CR are shown in Figure 1C-D.

All patients were followed for at least one year. Treatment responses and durations are shown in Figure 1E. By May 15, 2024, 17 out of 20 patients were alive. Of the 3 deaths, 1 patient with LA declined further therapy for financial constraints after neoadjuvant treatment and died a year later, another patient with LA refused maintenance therapy after surgery and died within a year, while one patient with LA died in a traffic accident four months post-radiotherapy. Among the all 20 patients, 5 (4 with LA and 1 with R) experienced local recurrence within 1 year. Of the 17 patients with R0 resection, 4 (3 with LA and 1 with R) had a local recurrence within 1 year.

Treatment Emergent Adverse Events (TEAEs) are summarized in Supplementary Tables S4-S5. All patients experienced at least one TEAE post-neoadjuvant therapy, primarily grades 1-2. Common TEAEs included alopecia

List of abbreviations: CAF, cancer associated fibroblast; CI, confidence interval; CNV, copy number variation; CR, complete response; DEG, differential expression gene; ECM, extracellular matrix; ESTIMATE, Estimation of STromal and Immune cells in MAlignant Tumour tissues using Expression data; FFPE, formalin fixed paraffin embedded; GSEA, gene set enrichment analysis; GSVA, gene set variation analysis; hdWGCNA, high-dimensional weighted gene co-expression network analysis; HNSCC, head and neck squamous cell carcinoma; LA, locally advanced; MIA, multimodal intersection analysis; mIHC, multiplex Immunohistochemistry; MPR, major pathological response; NMF, non-negative matrix factorization; ORR, objective response rate; OSCC, oral squamous cell carcinoma; pCR, pathological complete response; pEMT, part epithelial-mesenchymal transition; PR, partial response; PySCENIC, python-based single-cell regulatory network inference and clustering; RTK, receptor tyrosine kinase; scRNA-seq, single-cell RNA sequencing; ST, spatial transcriptomic; TAM, tumor-associated macrophage; TEAE, treatment emergent adverse event; TF, transcription factor; TKI, tyrosine kinase inhibitor; TME, tumor microenvironment; TP, paclitaxel and cisplatin.

[†]Qianting He, Shuojin Huang, and Dongxiao Tang made equal contributions to this work.

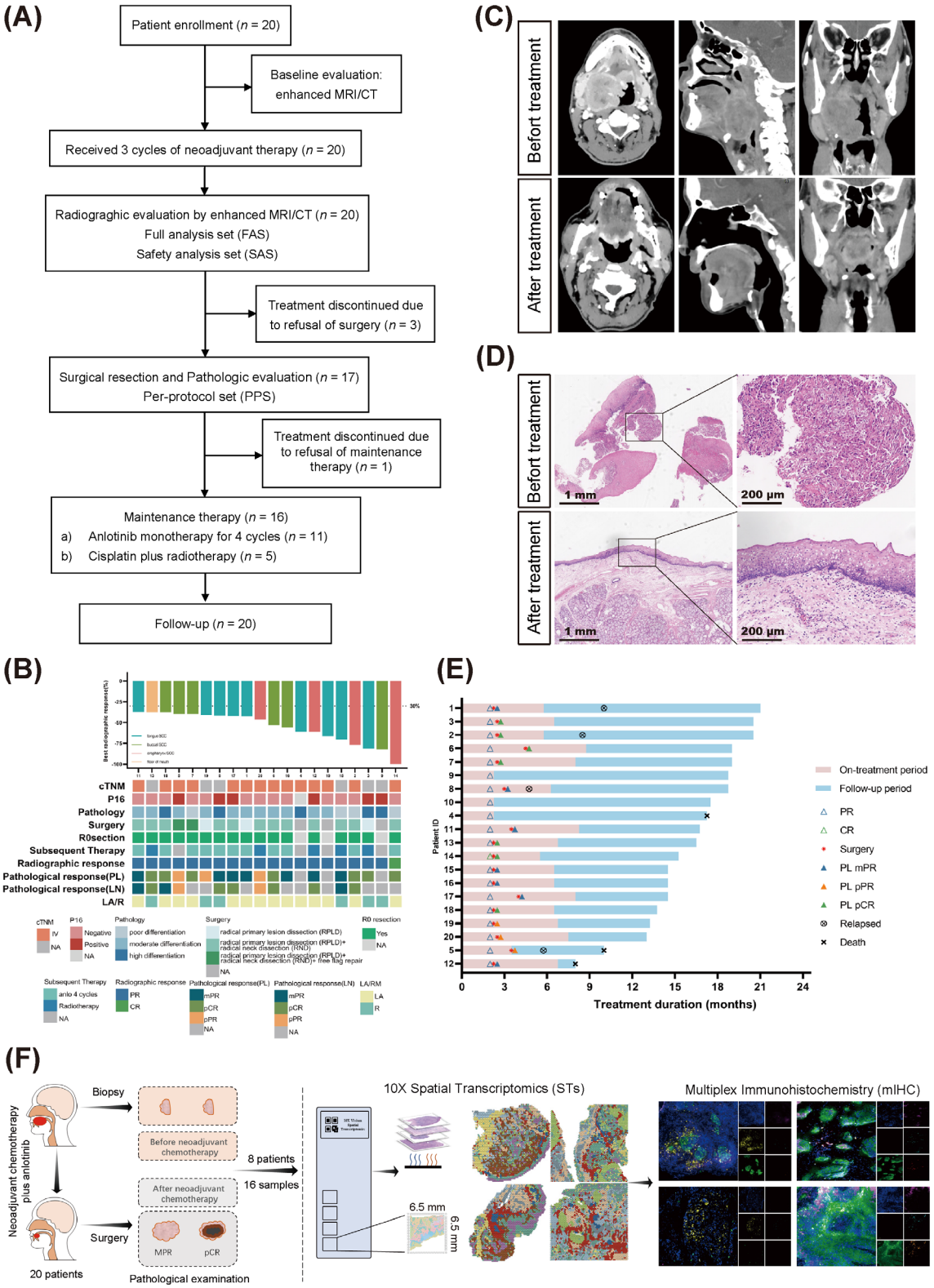

FIGURE 1 **Study trial design, treatment exposure, and survival analysis**. (A) Study flow chart depicting the trial design. A total of 20 patients were enrolled in the trial and received neoadjuvant therapy; 17 patients underwent surgical resection, and 16 patients received maintenance therapy. (B) Waterfall plot showing best radiographic response by RECIST 1.1, each bar represents one patient enrolled in the study ($n = 20$). Source data are available in the Supplementary Table S7. (C-D) Clinical radiographic and H&E-stained images of Patient #14 who achieved a CR. Scale bar, 200 μm. (E) Treatment exposure and response duration per RECIST v1.1 and pathological response ($n = 20$). The length of each bar represents the duration of treatment in each patient. (F) Illustration of the overall workflow for ST and mIHC. CR, complete response; ST, spatial transcriptomes; mIHC, multiplex immunohistochemistry

(100%), hypertension (90%), anemia (85%), and hand-foot syndrome (45%). Grade 3 TEAEs occurred in 50% of patients. No TRAEs caused drug discontinuation, dose reduction, death, or surgical delays.

To investigate the effects of neoadjuvant therapy on HNSCC, STs were conducted using Formalin Fixed Paraffin Embedded (FFPE) samples from 4 pCR and 3 non-pCR patients (Figure 1F, Supplementary Table S6). All 48,666 capture spots passed quality control, yielding a mean of 15,016 reads per spot (52.2 million per capture) and 4,498 mapped genes per sample.

Unsupervised clustering using the Louvain algorithm identified 10 niches across 14 samples (Supplementary Figure S1A), present in varying proportions (Supplementary Figure S1B). Each spot, containing 1-10 cells, was analyzed via multimodal intersection analysis (MIA) [5] with Single-cell RNA sequencing (scRNA-seq) datasets (GSE234933 and GSE181919). MIA predicted high malignant cell incidence in Niches 1, 4, and 6; Cancer Associated Fibroblasts (CAFs) in Niche 2; B cells and CAFs in Niche 3; endothelial cells and CAFs in Niches 5 and 7; immune cells in Niches 8 and 10; and ambiguous markers in Niche 9 (Supplementary Figure S1C). Manual annotation with cell type markers confirmed MIA results (Supplementary Figure S1D). Copy Number Variation (CNV) analysis showed recurrent chromosome 1 deletions and chromosome 3 amplifications in Niches 1, 4, and 6, aligning with prior studies [6]. Some Niche 1 spots exhibited low CNV, suggesting non-malignant squamous epithelial cells (Supplementary Figure S1E-F). Mapping niches onto FFPE sections revealed tumor regions comprised Niches 1, 4, and 6, with distinct spatial distributions: in addition to posttreatment samples of pCR patients, Niche 6 is primarily located at the tumor periphery, Niche 1 at the intermediate epithelial region, and Niche 4 at the leading edge. (Supplementary Figure S2). Estimation of STromal and Immune cells in MAlignant Tumour tissues using Expression data (ESTIMATE) analysis inferred tumor, stromal, and immune substructures, closely matching histological annotations (Supplementary Figure S3). Non-negative matrix factorization (NMF) [7] identified 11 transcriptional metaprograms, including a recurrent part Epithelial-Mesenchymal Transition (pEMT) module (COL17A1, LAMA3, and LAMC2), stress response genes (S100A9, S100A8, and KRT6A), and hypoxia-response genes (ENO1, DDIT4, and VEGFA; Supplementary Figure S4A-B. Other programs corresponded to CAF (ECM-CAFs: COL1A1, COL1A2, and COL3A1; myo-CAFs: DES, ACTN2, and MYH2) and immune lineages. NMF results aligned with niche classifications (Supplementary Figure S4C-D).

To further examine treatment effects on HNSCC, we analyzed niche compositions before and after treatment. Posttreatment samples showed significant decreases in Niche 4 and Niche 6 (Niche 4: 23.9% to 2.8%; Niche 6: 13.4% to 5.2%), reflecting a robust anti-tumor effect (Supplementary Figure S5A). Conversely, Niche 3, 5, 7, and 8 increased posttreatments (Niche 3: 6.9% to 16.9%; Niche 5: 7.6% to 13.4%; Niche 7: 4.7% to 7.3%; Niche 8: 2.1% to 8.3%). Gene Set Variation Analysis (GSVA) analysis revealed upregulated mRNAs in posttreatment samples enriched in pathways related to B cell receptor signaling, complement action, and adaptive immune response, while downregulated mRNAs were linked to epidermis development and cell cycle regulation (Supplementary Figure S5B). Niche 3, primarily composed of B cells and CAFs (Supplementary Figure S1C), was located near tumor niches (Supplementary Figure S2), suggesting interactions with tumor cells. Transcriptomic analysis showed that pretreatment Niche 3 was associated with extracellular matrix (ECM) markers (e.g., COL7A1 and DSP), while posttreatment samples displayed upregulation of immune regulatory genes and B cell activation markers (e.g., IGHG3, IGLC1, SFRP2, and SFPR4; Supplementary Figure S5C). Gene Set Enrichment Analysis (GSEA) confirmed enrichment of immune response and B cell-mediated immunity gene sets in posttreatment Niche 3 (Supplementary Figure S5D). CellChat analysis revealed increased communication strength between Niche 3 and tumor niches (Niche 1, 4, and 6) after treatment (Supplementary Figure S5E-F). Ligand-receptor pairs (C3-ITGAX + ITGB2, CCL5-ACKR1, and SEMA3C-PLXND1) were significantly upregulated posttreatment, suggesting their role in anti-tumor immunity (Supplementary Figure S5G). Flow pattern showed dominant SEMA3, CCL, ANGPTL, and COMPLEMENT signaling pathways posttreatment, whereas VEGFA, VISFATIN, NRG, and ncWNT were predominant pretreatment (Supplementary Figure S5H).

To delineate key molecular characteristics of non-pCR samples, we manually selected spots from residual tumors (Supplementary Figure S6A) and identified an insensitive signature score via Differential Expression Gene (DEG) analysis between residual tumor cells and other niches (Supplementary Figure S6B-C). GSEA revealed upregulated genes enriched in pathways, such as oxidative phosphorylation, MYC targets, DNA repair, and interferon alpha response (Supplementary Figure S6D-E). Using high-dimensional Weighted Gene Co-expression Network Analysis (hdWGCNA), we identified seven gene modules, with Module RN4 showing the highest positive correlation to the insensitive score (Supplementary Figure S6F-H). Python-based Single-Cell Regulatory Network Inference and Clustering (PySCENIC) analysis revealed differentially activated transcription factors (TFs), including HES1, FOXQ1, and FOXA1, in the insensitive niche (Supplementary Figure S6I).

Notably, FOXQ1 was consistently identified across datasets and was significantly enriched in naïve non-pCR samples compared to naïve pCR samples, suggesting its key role in tumor cell insensitivity (Supplementary Figure S7A-B). To explore interactions between insensitive niches and the Tumor Microenvironment (TME), Squidpy analysis revealed a positive spatial association with Niche 10, predominantly composed of immune cells like Tumor-associated Macrophages (TAMs) and T cells (Supplementary Figure S7C). Immune suppressors such as CCL18 showed elevated expression in non-pCR patients, indicating complex TME interactions (Supplementary Figure S7D-E). Higher CCL18 expression was detected in Niche 10, with increased CCL18-PITPNM3 signaling between Niches 10 and 1, 4, 6 in non-pCR patients (Supplementary Figure S7F-G). Further investigation revealed FOXQ1 and CCL18 expression significantly enriched in non-pCR patients, particularly post-neoadjuvant therapy (Supplementary Figure S8A-B). $CD206^+/CCL18^+$ TAMs were predominantly located near $FOXQ1^+$ tumor cells, suggesting localized immunosuppressive interactions (Supplementary Figure S8A).

In this study, oxidative phosphorylation and FOXQ1 expression were enriched in residual tumor cells post-neoadjuvant therapy. FOXQ1, an oncogenic transcription factor, promotes complex I-linked oxidative phosphorylation by upregulating NDUFS1 and NDUFV1 [8]. $CD206^+/CCL18^+$ TAM density differed significantly between pCR and non-pCR patients, and these TAMs were spatially near $FOXQ1^+$ tumor cells. CCL18, a key chemokine in tumor biology, induces regulatory T cell recruitment and a pro-tumor M2-like macrophage phenotype [9]. It also promotes cancer progression via metastasis and EMT through its receptor PITPNM3 [10]. The interaction between $FOXQ1^+$ tumor cells and $CD206^+/CCL18^+$ TAMs needs further study.

In conclusion, the combination of anlotinib with TP neoadjuvant therapy demonstrates high clinical efficacy and a favorable safety profile in patients with resectable HNSCC. And further high-quality, multi-center, double-blind phase III RCTs with longer follow-up are needed to validate anlotinib's potential in a larger HNSCC population.

AUTHOR CONTRIBUTIONS

Conceptualization: Shuojin Huang, Qianting He, Dongxiao Tang, Wanhang Zhou, Congyuan Cao, Anxun Wang, and Demeng Chen. Methodology: Shuojin Huang, Qianting He, Dongxiao Tang, Wanhang Zhou, and Congyuan Cao. Data analysis and curation: Shuojin Huang, Wanhang Zhou, Rongsong Ling, Jie Chen, and Bokai Yun. Investigation and validation: Shuojin Huang, Qianting He, Dongxiao Tang, Wanhang Zhou, Congyuan Cao, Xin Zheng, and Yanchen Li. Resources: Jie Chen, Anxun Wang, and Demeng Chen. Writing-original draft: Shuojin Huang, Wanhang Zhou, Anxun Wang, and Demeng Chen. Writing-review & editing: Anxun Wang and Demeng Chen. Supervision and funding acquisition: Anxun Wang and Demeng Chen.

ACKNOWLEDGEMENTS

Not applicable.

CONFLICT OF INTEREST STATEMENT

The authors declare no competing interests.

ETHICS APPROVAL AND CONSENT TO PARTICIPATE

The ethical, medical, and scientific aspects of the research were reviewed and approved by the Ethics Committee of the First Affiliated Hospital, Sun Yat-Sen University before initiation (Ethical approval number: [2022]474), and the trial was registered at the Chinese Clinical Trial Registry (ChiCTR2300078009).

FUNDING INFORMATION

This work was supported by funding from the National Natural Science Foundation of China (No. 82173041, 82372868, 82173362, 81872409, 82304069, 82403184, and 823B2079), Guangzhou Municipal Science and Technology Bureau (No. 2024B03J1384), China Postdoctoral Science Foundation (No. 2023M734003), Natural Science Foundation of Guangdong Province (No. 2024A1515012316), and Basic and Applied Basic Research Foundation of Guangdong Province (No. 2023A1515110475).

DATA AVAILABILITY STATEMENT

The raw data for Spatial Transcriptomics sequencing in this study are uploaded to the Genome Sequence Archive with accession ID HRA007551. Processed scRNA-seq data from the external dataset are available through the Gene Expression Omnibus (GEO) under accession number GSE234933 and GSE181919.

Qianting He[1,†]
Shuojin Huang[1,†]
Dongxiao Tang[2,†]
Congyuan Cao[1]
Wanhang Zhou[1]
Rongsong Ling[3]
Jie Chen[4]
Bokai Yun[5]
Xin Zheng[1]
Yanchen Li[1]
Anxun Wang[1]
Demeng Chen[3]

[1]*Department of Oral and Maxillofacial Surgery, The First Affiliated Hospital, Sun Yat-Sen University, Guangzhou, Guangdong, P. R. China*
[2]*Department of Stomatology, The Third Affiliated Hospital, Sun Yat-Sen University, Guangzhou, Guangdong, P. R. China*
[3]*State Key Laboratory of Oncology in South China, Center for Translational Medicine, the First Affiliated Hospital, Sun Yat-Sen University, Guangzhou, Guangdong, P. R. China*
[4]*Department of Orthodontics, Hospital of Stomatology, Guangdong Provincial Key Laboratory of Stomatology, Guanghua School of Stomatology, Sun Yat-Sen University, Guangzhou, Guangdong, P. R. China*
[5]*Department of Oral and Maxillofacial Surgery, Hospital of Stomatology, Guangdong Provincial Key Laboratory of Stomatology, Guanghua School of Stomatology, Sun Yat-Sen University, Guangzhou, Guangdong, P. R. China*

Correspondence
Demeng Chen; State Key Laboratory of Oncology in South China, Center for Translational Medicine, The First Affiliated Hospital, Sun Yat-Sen University, Guangzhou, 510060, Guangdong, P. R. China.
Email: chendm29@mail.sysu.edu.cn

Anxun Wang; Department of Oral and Maxillofacial Surgery, The First Affiliated Hospital, Sun Yat-Sen University, 58 Zhongshan Er Road, Guangzhou, 510080, Guangdong, P. R. China.
Email: wanganx@mail.sysu.edu.cn

ORCID

Rongsong Ling https://orcid.org/0000-0002-0402-9818
Anxun Wang https://orcid.org/0000-0003-2249-7356
Demeng Chen https://orcid.org/0000-0001-7230-2495

REFERENCES

1. Mody, MD, Rocco, JW, Yom, SS, Haddad, RI, Saba, NF. Head and neck cancer. Lancet. 2021;398(10318), 2289-99.
2. Shen, G, Zheng, F, Ren, D, Du, F, Dong, Q, Wang, Z, et al. Anlotinib: A novel multi-targeting tyrosine kinase inhibitor in clinical development. J Hematol Oncol. 2018;11(1), 120.
3. Huang, Z, Su, Q, Li, W, Ren, H, Huang, H, Wang, A. Suppressed mitochondrial respiration via NOX5-mediated redox imbalance contributes to the antitumor activity of anlotinib in oral squamous cell carcinoma. J Genet Genomics. 2021;48(7), 582-94.
4. Li, S, Cao, C, Huang, Z, Tang, D, Chen, J, Wang, A, et al. SOD2 confers anlotinib resistance via regulation of mitochondrial damage in OSCC. Oral Dis. 2024;30(2), 281-91.
5. Moncada, R, Barkley, D, Wagner, F, Chiodin, M, Devlin, JC, Baron, M, et al. Integrating microarray-based spatial transcriptomics and single-cell RNA-seq reveals tissue architecture in pancreatic ductal adenocarcinomas. Nat Biotechnol. 2020;38(3), 333-42.
6. Puram, SV, Tirosh, I, Parikh, AS, Patel, AP, Yizhak, K, Gillespie, S, et al. Single-Cell Transcriptomic Analysis of Primary and Metastatic Tumor Ecosystems in Head and Neck Cancer. Cell. 2017;171(7), 1611-24. e24.
7. Greenwald, AC, Darnell, NG, Hoefflin, R, Simkin, D, Mount, CW, Gonzalez Castro, LN, et al. Integrative spatial analysis reveals a multi-layered organization of glioblastoma. Cell. 2024;187(10), 2485-501. e26.
8. Kim, SH, Singh, SV. The FoxQ1 transcription factor is a novel regulator of electron transport chain complex I subunits in human breast cancer cells. Mol Carcinog. 2022;61(3), 372-81.
9. Cardoso, AP, Pinto, ML, Castro, F, Costa, AM, Marques-Magalhaes, A, Canha-Borges, A, et al. The immunosuppressive and pro-tumor functions of CCL18 at the tumor microenvironment. Cytokine Growth Factor Rev. 2021;60, 107-19.
10. Chen, J, Yao, Y, Gong, C, Yu, F, Su, S, Chen, J, et al. CCL18 from tumor-associated macrophages promotes breast cancer metastasis via PITPNM3. Cancer Cell. 2011;19(4), 541-55.

SUPPORTING INFORMATION

Additional supporting information can be found online in the Supporting Information section at the end of this article.